Study of the Influence of Substrate Topography on the Focusing Performance of Advanced Lithography Scanners

Bruno La Fontaine[*a], Jan Hauschild[**b], Mircea Dusa[b], Alden Acheta[a], Eric Apelgren[a],
Marc Boonman[b], Jouke Krist[b], Ashok Khathuria[a], Harry Levinson[a], Anita Fumar-Pici[b],
Marco Pieters[b]

[a]Advanced Micro Devices; [b]ASML

ABSTRACT

A Phase-Grating Focus Monitor (PGFM) is used to assess the focus control of a state-of-the-art lithography scanner (TWINSCAN™ AT:1100) over substrate topography. The starting wafer flatness quality is found to be critical in minimizing the overall defocus distribution. In fact, on nearly all wafers, the most significant contributor to defocus across the wafer was the small-scale topography. Results obtained over programmed topography, created by etching various patterns into silicon, are found to agree well with the simulated defocus behavior based on the measurement of the wafer surface obtained on the scanner metrology stage. Finally, we report on preliminary focus control results over realistic device-type substrate topography, involving thin-film and polish effects.

Keywords: Topography, Phase-Grating Focus Monitor, Phase-Shift Focus Monitor, TWINSCAN, and Non-Correctable Focus Errors (NCE),

1. INTRODUCTION

As the dimensions of devices shrink and lithographers use scanners with increasing numerical aperture and shorter actinic wavelength, the useable depth of focus keeps getting smaller and smaller [1, 2]. Nowadays, certain processes may be based on depths of focus around 250 nm. In order to maintain process capability, one needs to be able to characterize the distribution of defocus on the wafer with high sensitivity and good repeatability, in order to minimize any errors contributing to the focus budget.

The Phase-Shift Focus Monitor (PSFM) [3-5] and Phase-Grating Focus Monitor (PGFM) [6] provide a means of evaluating very precisely across-wafer focus distributions. In this study, we use these focus monitors to characterize the contribution of different types of substrates to the entire focus distribution, for sub-100-nm processes using state-of-the-art 193-nm lithography scanner. We then compare these results with the focus behavior predicted by the scanner (simulated defocus), which is based on the capability of this dual-stage scanner to measure substrate topography and correct for initial wafer flatness using complex compensation algorithms.

2. DESCRIPTION OF THE EXPERIMENTS

All experiments are performed on an ASML TWINSCAN™ AT:1100 scanner (0.75NA, 193nm), using three different types of substrates: (i) bare silicon wafers, (ii) silicon wafers with etched areas of various sizes and depths, and (iii) wafers that mimic substrates encountered in production when patterning the gate of a transistor. In each case, we first measure the wafer topography or flatness using the TWINSCAN™ metrology stage, and then we measure the wafer focus distributions using the focus monitors (PGFM and/or PSFM). In the following sub-sections, we describe briefly

---

[*] bruno.lafontaine@amd.com; phone 1 (408) 749-2060; fax 1 (408) 774-8813; http://www.amd.com; Advanced Micro Devices, One AMD Place, m/s 78, PO Box 3453, Sunnyvale, CA 94088-3453;

[**] jan.hauschild@asml.com; phone 31 (40) 268-5535; fax 31 (40) 268-5577; http://www.asml.com; ASML, De Run 1110, 5503 LA Veldhoven, The Netherlands;

the measurement techniques and the basic principles of leveling used by the scanner. The last sub-section describes the conditions used for the experiments.

2.1 The focus monitors (PGFM and PSFM)

The focus monitor patterns used in the present study have been described in a previous publication [6]. The basic operating principle of the PSFM is that the aerial image of a line with a 90º-phase patch on one of its sides tends to move toward this patch when there is a positive defocus and away from it for negative defocus. Since the lines and phase patches are arranged to form concentric boxes, any focus error is translated into an alignment error that can be measured with an overlay metrology tool. A linear relation of the measured overlay as a function of programmed defocus is then used to quantitatively evaluate any focus errors.

The PGFM is based on the same idea of converting focus errors into alignment errors and measuring them with an overlay metrology tool. However, the isolated lines with the large 90º phase patches used for the PSFM are replaced by phase gratings [7], which generate the equivalent of a two-beam interferometer inside the lens and are very sensitive to focus errors.

2.2 Basic principles of scan leveling employed by the AT:1100

The TWINSCAN™ AT:1100 dual-stage system enables parallel measuring and exposing of a wafer as is schematically depicted in Figure 1. In the measurement position, a three-dimensional map of the wafer surface is generated using a high-spatial-frequency level sensor.[8] This wafer map has a spatial resolution of 2.8 mm × 0.5 mm, which is obtained by using level sensor spots that have a dimension of 2.8 mm × 2.5 mm and over sampling in the scan direction. The high-resolution map of the wafer enables the optimization of the leveling profiles for the exposure slit size.
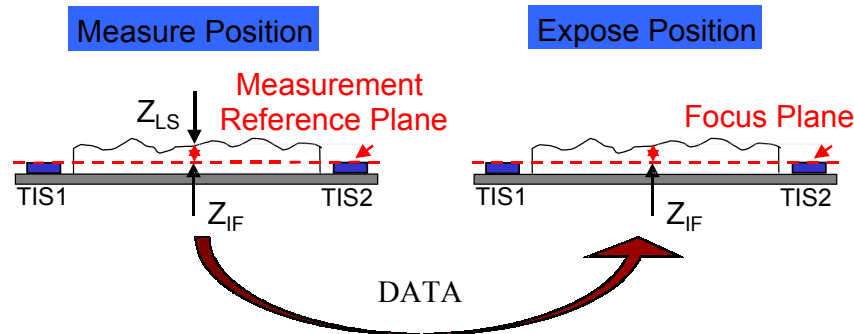

Figure 1 – Principle of the dual-stage leveling technology.

We define the wafer non-correctable focus errors, NCE, as the wafer surface topography that cannot be completely compensated due to the finite size of the exposure slit. For a static exposure, these non-correctable errors correspond directly to defocus errors. However, during a scanned exposure, the non-correctable errors change continuously as the slit is scanned over a particular position on the wafer. In the latter case, the average value of the non-correctable errors over the exposure time defines the average defocus that this position experiences during the exposure. We define this value that depends on the slit size and on the spatial-frequency and amplitude of the wafer topography as simulated defocus, or as the Moving Average in the z-direction (MA(z)). Changes in the topography that are larger then the slit dimensions can be leveled by adjusting the stage height and tilt angle accordingly. If the topography variation occurs over distances that are smaller than the slit dimensions, the height changes cannot be leveled effectively.

2.3 Experimental conditions

For the experiments reported in this paper, we use an ASML ArF step-and-scan system, the TWINSCAN™ AT:1100, which has a numerical aperture of 0.75. We use a conventional illumination setting with $\sigma = 0.326$. We use PAR735 resist on an AR19 anti-reflective coating, with an exposure dose of 22.0 mJ/cm^2 for PGFM and 26.5 mJ/cm^2 for PSFM.

The PGFM and PSFM data are measured using either a KLA5200 or an Archer overlay tool. The PGFM reticle has 221 focus-detection patterns, or measurement sites, with box-in-box patterns made of 500-nm-period phase-shift gratings. The PSFM reticle has 77 measurement sites, with box-in-box patterns made of 140-nm isolated lines. The results are analyzed and displayed using the Weir software [9] and other computer routines developed internally.

3. RESULTS AND ANALYSIS

In this section, we present the results from the PGFM and PSFM focus monitors, as well as the metrology results from the AT:1100. We also compare the simulated defocus behavior of the scanner with that observed with PGFM and PSFM.

3.1 Focus distributions on bare silicon wafers

In order to evaluate the influence of the wafer flatness quality, we select 12 wafers from four groups corresponding to different wafer fabrication processes (wafers with different flatness or topography specification). The flatness of these wafers is first characterized by a capacitive gauge sensor with a 4-mm head and the range of deviation from the best plane-fit over areas of 25 mm × 25 mm, as defined as Site flatness Front side least sQuare fit Range (SFQR), is reported for each areas. We then use the sum of the mean value and three times the standard deviation (mean + 3σ) of the SFQR for all fields on a wafer, excluding a 3-mm zone at the edge of the wafer, to describe the overall flatness of these wafers.

Next, the PGFM reticle is exposed at constant focus on 37 fields measuring 26 mm × 32 mm and the placement offsets of the patterns printed on the wafers are measured using an overlay metrology tool. Wafer focus distribution as measured by the overlay tool is analyzed with commercial software [8] in order to extract the focus offsets across the whole wafer as well as to evaluate systematic and residual components of focus distributions across the scanner's image field. The standard deviation of the defocus data measured by PGFM is then compared to the initial wafer flatness (described by SFQR).

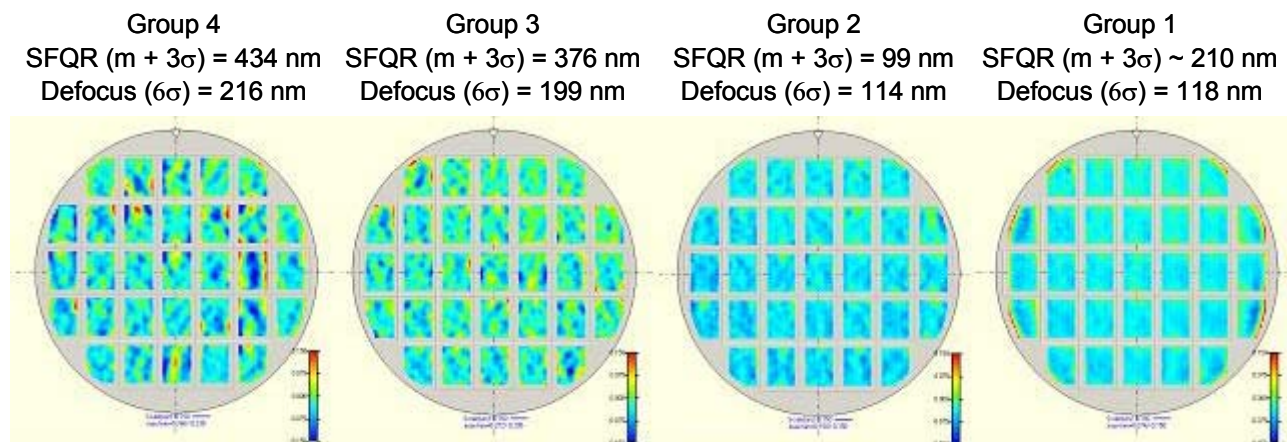| Group 4	Group 3	Group 2	Group 1
SFQR (m + 3σ) = 434 nm	SFQR (m + 3σ) = 376 nm	SFQR (m + 3σ) = 99 nm	SFQR (m + 3σ) ~ 210 nm
Defocus (6σ) = 216 nm	Defocus (6σ) = 199 nm	Defocus (6σ) = 114 nm	Defocus (6σ) = 118 nm

Figure 2 – PGFM focus distribution using a constant-focus exposure, on four wafers of different flatness quality. The color bar indicates the defocus magnitude in units of microns. The four wafer groups correspond to different wafer fabrication processes, qualified using the mean + 3σ value of the SFQR over all fields on each wafer.

Figure 2 illustrates the effects of wafer flatness characteristics on the focus distribution as measured by PGFM. It is obvious from the contour maps presented in figure 2, that the high-spatial-frequency topography of the wafer contributes most of the defocus distribution and that a significant improvement in defocus can be obtained by using better quality wafers (e.g., from group 2). It is also interesting to note that although the group 1 wafers seem to have less high-frequency topography, their flatness value and measured defocus distribution are larger than those of group 2. This can be attributed almost exclusively to topography at the periphery (edge), where the wafer surface appears to *curl up*. If

these fields were not considered in the analysis, then the wafers in Group 1 would have the best defocus distribution with a standard deviation of less than 19 nm ($6\sigma \sim 100$ nm).

The comparison of total defocus to wafer flatness is summarized on the graph in figure 3, which shows good correlation between the wafer defocus distribution and the wafer flatness distribution. These data provide the basis for deciding which type of wafer to use for a specific product (with its own focus budget) when using a certain scanner. Figure 4 contains two sets of data, one that has been generated on an older-generation, single-stage scanner [6], while the other one was obtained on the TWINSCAN™ AT:1100 dual-stage ArF scanner. Examination of Fig. 4 illustrates clearly the progress in scanner focus control achieved by mapping the wafer surface on the metrology stage before applying the appropriate compensation on the exposure stage. From this graph, one can also appreciate the importance of using flat wafers in order to minimize the wafer topography contribution to the total focus budget. For the earlier tool, the use of wafers with a flatness of approximately 350 nm (mean + 3σ SFQR) could contribute up to about 40% of the total distribution of defocus. In addition, the residual errors for that tool (if one would use extremely flat wafers) could contribute between 200 and 250 nm to the total focus distribution across the entire wafer. For the TWINSCAN™ AT:1100, the wafer flatness is the main contributor, even for the flattest wafers used in this study. In fact, as we will show, the tool contribution after subtracting systematic errors (e.g., due to the reticle characteristics) is of the order of 10 nm rms.
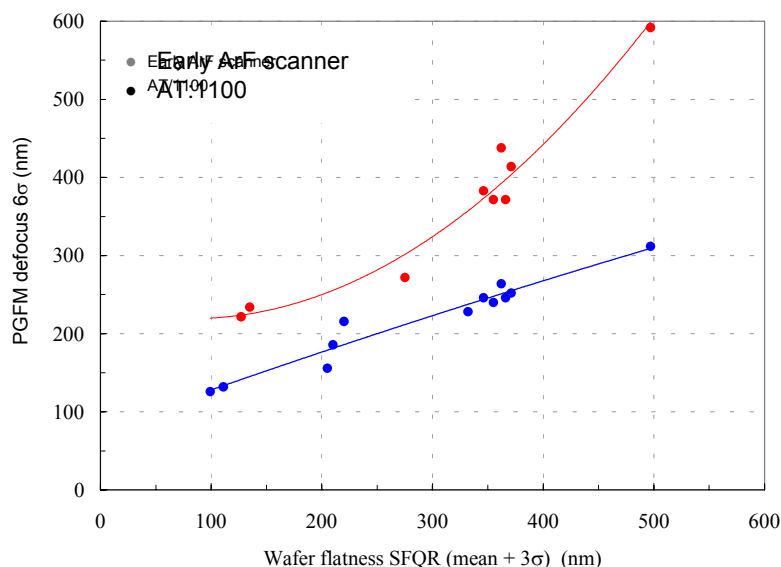

Figure 3 – Influence of wafer flatness on the observed focus distribution across the wafer. The wafer quality is expressed in terms of the SFQR distribution of the wafer and estimated using the mean plus three standard deviations value of this SFQR distribution. The observed focus distribution is expressed in terms of its six standard deviations value of the defocus data measured with PGFM/PSFM. The red dots correspond to 6σ value of the distribution of defocus for an early ArF scanner after correcting for systematic errors and the blue dots represent the 6σ value of the raw distribution of defocus for the TWINSCAN™ AT:1100.

A more detailed analysis of the focus distribution follows, based on the PGFM measurements and on the surface maps obtained on the scanner metrology stage.

First, let us consider a wafer from group 3, characterized by SFQR (mean + 3σ) = 332 nm. The raw defocus data obtained with PGFM are shown in figure 4(a), the average field defocus data appear in figure 4(b), and the residual defocus data, obtained by subtracting the average field data from the raw data, are displayed in figure 4(c). The full wafer map of raw defocus data has a distribution characterized by a standard deviation of 34.5 nm. The average field distribution of defocus is obtained by averaging all data points across the wafer corresponding to identical field

locations. Its distribution has a standard deviation of 12.9 nm. The residual defocus map has a standard deviation of 32.1 nm.
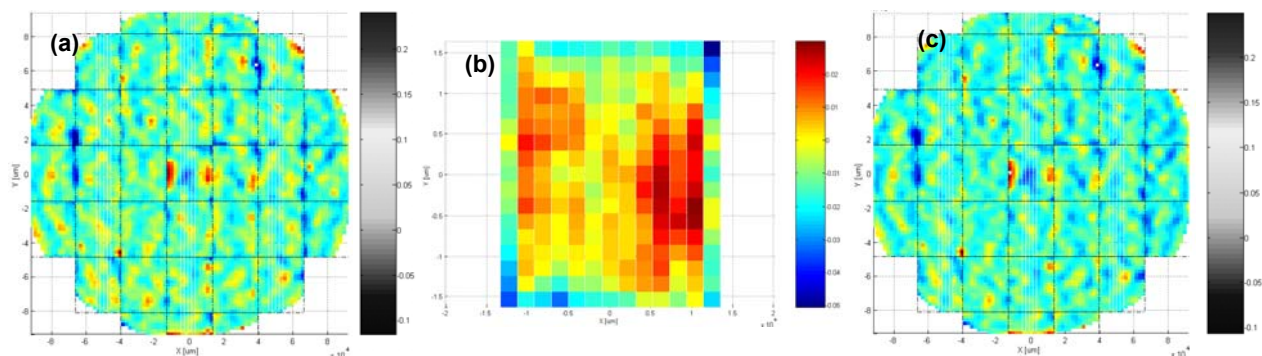

Figure 4 – Raw defocus data obtained with PGFM on a group-3 wafer, expressed in μm. (a) The full wafer map of raw defocus data has a distribution characterized by a standard deviation of 34.5 nm (b) The average field distribution of defocus is obtained by averaging all data points across the wafer corresponding to identical field locations. Its distribution has a standard deviation of 12.9 nm. (c) The residual defocus wafer map is obtained by subtracting the average-field data from the raw defocus wafer map. Its distribution has a standard deviation of 32.1 nm.

The map for this wafer measured on the metrology stage of the TWINSCAN™ AT:1100 is shown in figure 5(a). The simulated defocus (MA(z)) based on this wafer map is displayed in figure 5(b). The map of the difference between the residual defocus measured by PGFM and the simulated defocus is plotted in figure 5(c). The wafer topography, after subtracting the best-fit global plane has a 75-nm rms distribution. The simulated defocus distribution has a standard deviation of 31 nm. The difference between the defocus data measured with PGFM and the simulated defocus (MA(z)) is characterized by a standard deviation of only 12.5 nm, indicating a very close agreement between the actual scanner performance, as measured with PGFM, and the best possible performance of the scanner based on the measured wafer topography on the TWINSCAN™ AT:1100. We would also like to note that this particular wafer is characterized by a depression in the central field, as can be seen on the map displayed in figure 5(a), which is the origin of the defocus behavior measured with PGFM in the central field (figure 4(a)) and also predicted by simulating the defocus distribution for this field (figure 5(b)).
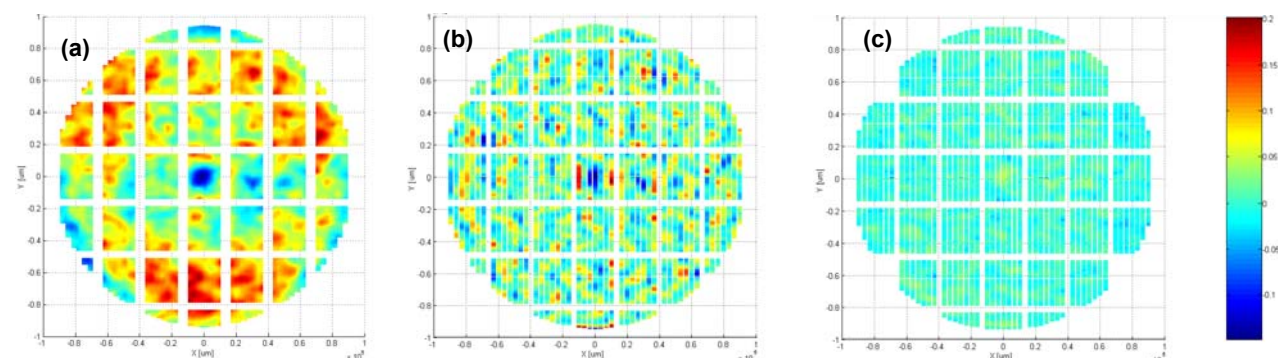

Figure 5 – (a) Contour map of the wafer measured on the stage at the measurement position of the TWINSCAN™ AT:1100, for a wafer of group 3. The wafer topography, after subtracting the best-fit global plane has a 75-nm rms distribution. (b) Simulated defocus map. The simulated defocus distribution across the wafer has a standard deviation of 31 nm. (c) The difference between the defocus data (as shown in figure 4c) and the simulated defocus is characterized by a standard deviation of only 12.5 nm. The data presented here are all expressed in μm. A very close agreement is observed between the actual scanner performance and the best possible performance of the scanner, based on the metrology performed on the TWINSCAN™ AT:1100.

A similar analysis is performed for a flatter wafer from group 2, with SFQR (mean + 3σ) = 99 nm. For this wafer, the residual defocus data, which has a standard deviation of 15.9 nm, is presented in figure 6(a). The simulated defocus distribution based on the metrology stage has a standard deviation of 14.8 nm and is displayed in figure 6(b). The difference between the actual defocus measurements and the simulated defocus is plotted in figure 6(c) and is characterized by an rms error of only 8.5 nm.
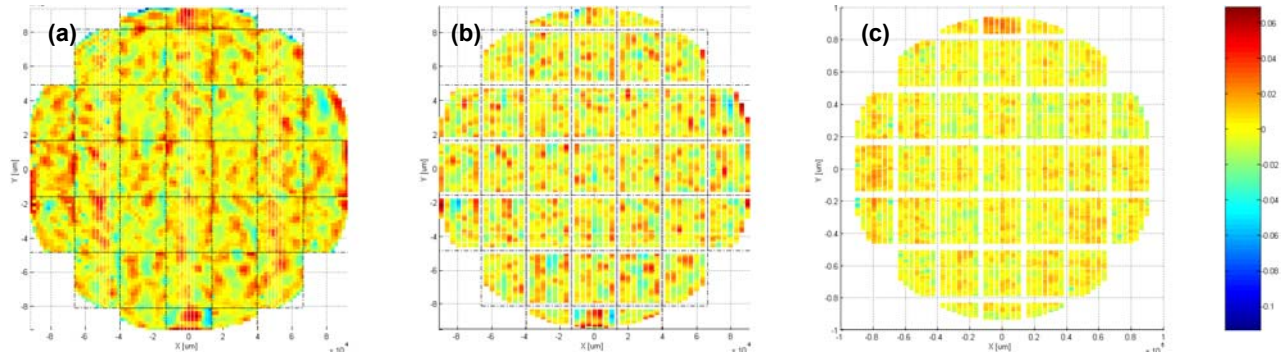

Figure 6 – Contour maps of the measured defocus and the simulated defocus for a wafer of group 2, expressed in μm. (a) The residual defocus wafer map has a distribution with a standard deviation of 15.9 nm. (b) The simulated defocus distribution has a standard deviation of 14.8 nm. (c) The difference between the defocus data measured by PGFM and the simulated defocus (MA(z)) is characterized by a standard deviation of 8.5 nm.

In table 1, an overview of the results is given for one wafer out of each group. All values given are the averages over the values per field. The PGFM results, corrected for average field (or systematic) errors, match the simulated defocus nearly one to one. One can also observe this close agreement in figure 7. From these results, one can conclude that even for the flattest wafer used in this experiment, the wafer topography dominates the defocus distribution.

	Group 4	Group 3	Group 2	Group 1
SFQR (mean+3σ) 25mm x 25 mm [nm]	434	376	99	-
SFQR (mean) 25mm x 25 mm [nm]	192	154	66	-
PGFM defocus 6σ [nm]	216	199	114	118
PGFM defocus 6σ [nm] after correction	199	185	90	85
Simulated defocus [MA(z)] 6σ [nm]	197	179	88	-

Table 1 – Comparison of wafer flatness as measured by the wafer manufacturer, the resulting defocus distribution on the TWINSCAN™ AT:1100 with and without intrafield correction, as well as the simulated defocus based on the wafer map measured by the TWINSCAN™ AT:1100 All values given are the averages over the values per field.
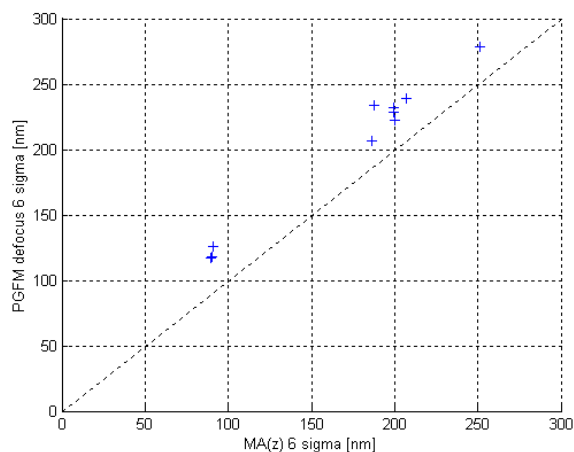
Figure 7 – Defocus values measured using PGFM as a function of the simulated defocus MA(z), based on the wafer maps measured by the TWINSCAN™ AT:1100. Note the excellent correlation and the small difference between the defocus measurements and the simulated defocus (about 20 nm), which is mainly due to the intrafield contribution..

3.2 Focus control over programmed topography

In this sub-section, we investigate the effect of programmed topography on focus control. The programmed topography has been created by etching patterns with various spatial frequency and different etch depths into bare silicon wafers. The wafer layout used is shown in figure 8, together with the vector plot of the PGFM data obtained on such a wafer that is etched to a depth of 178 nm. The PGFM data are obtained at the nominal best focus of the scanner.

We focus our analysis on the fields with topography varying along the scan direction because the scanner can partially correct for this kind of topography. We group the PGFM data from similar fields and average them in order to improve the signal-to-noise ratio.
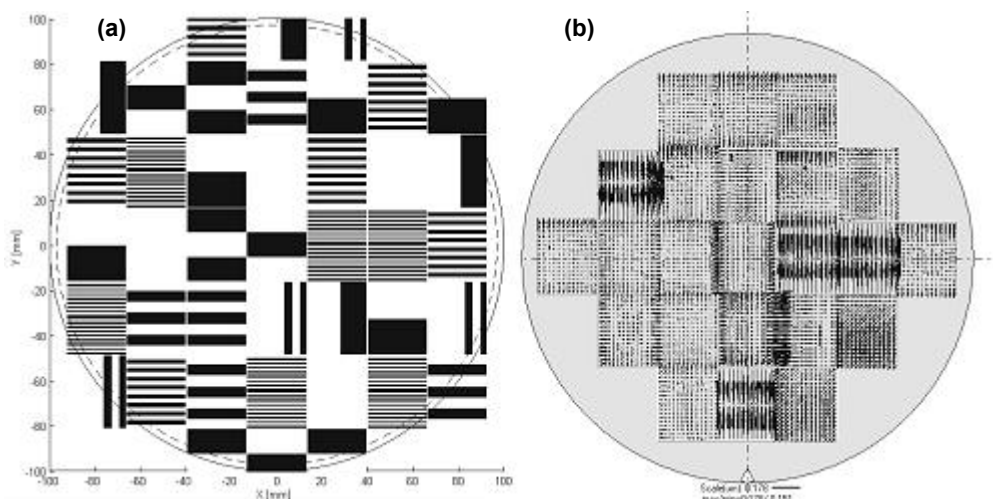

Figure 8 – (a) Wafer distribution of scanner fields with various etched patterns (b) Vector plot of the PGFM data obtained on this type of substrate, with an etch depth of 178 nm.

Typical results for etched patterns that are 10.6 mm and 1.9 mm long (in the scan direction) are displayed in figures 9 and 10. The PGFM measurement loci relative to the etched patterns are depicted schematically on the left side of the figures. The defocus contour map from the PGFM data is plotted in the center part. A lineout of the defocus along the scanning direction and averaged over the slit width is shown on the right side of the figures. In this lineout, the programmed etch step, the measured wafer map by the TWINSCAN™ AT:1100 and the simulated defocus based on the wafer map are also shown.
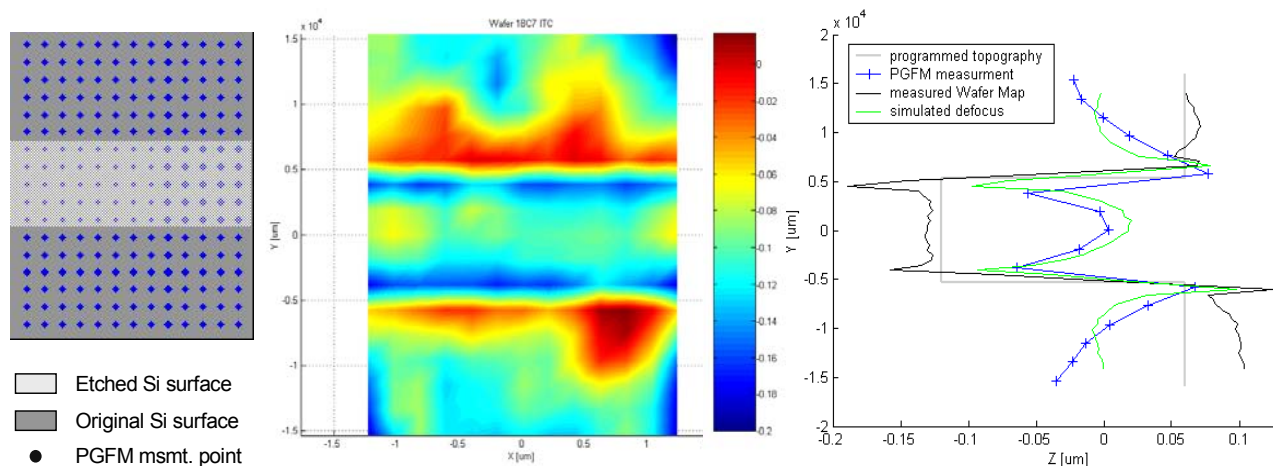

Figure 9 – PGFM results obtained over a field with programmed topography consisting of a central etched area that is approximately 10.6 mm long (in the scan direction) and 180 nm deep. The defocus values are expressed in μm. The predicted performance matches the PGFM results very well.
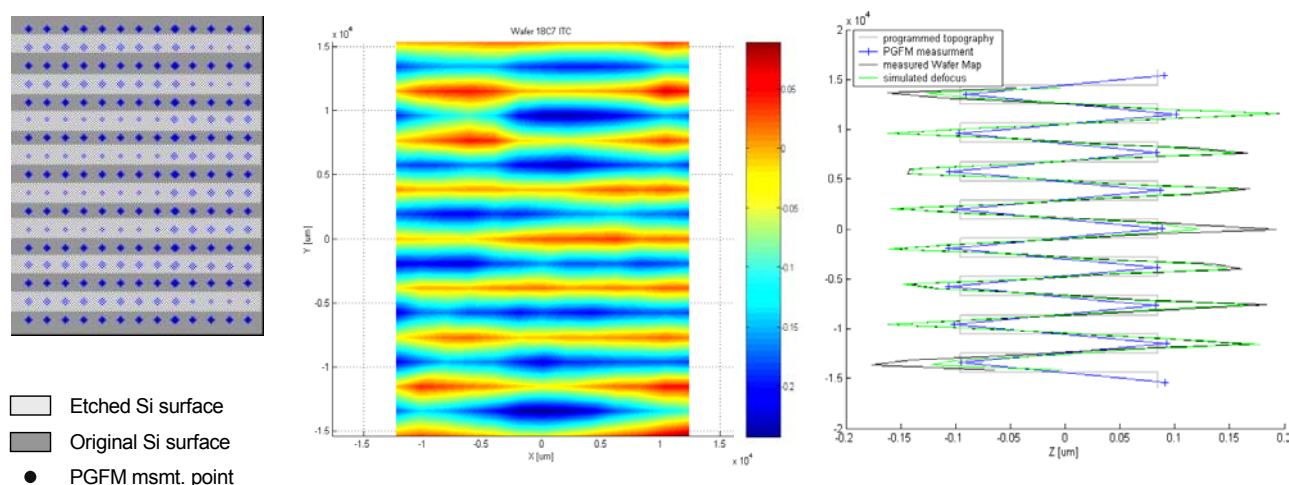

Figure 10 – PGFM results obtained over a field with programmed topography consisting of etched areas that are approximately 1.9 mm long (in the scan direction) and 180 nm deep. The defocus values are expressed in μm. Here again, the predicted performance matches the PGFM results very well.

These two relatively extreme cases illustrate the fact that the scanner is able to correct for slowly varying topography in the scan direction (see figure 9). Leveling and focusing over fields with rapidly varying topography are achieved by averaging the height differences within the slit rather then by following the topography (see figure 10).

The results of different programmed topographies, for etch depths of 180 nm and 38 nm, are summarized in figure 11. The PGFM results are compared to the simulated defocus based on the measured wafer map as function of the spatial

extent of the etched areas. The height leveling transfer function, given a finite slit size, is also plotted in this figure. The transfer function qualitatively shows why the topography cannot be leveled for etch lengths that are smaller than a certain fraction of the slit dimension.

The behavior for the different etch depths is the same except for a scaling factor. The PGFM data correlates well with the simulated defocus except for spatial extents smaller than 2 mm, where the measured wafer map is averaged due to the spot size of the level sensor. For the 180-nm etch depth, the PGFM measurement point for a spatial etch extent of 4.8 mm is better than predictions and the transfer function would suggest, which might be due to etch non-uniformity across the wafer and across the field. The defocus noise level induced by wafer roughness can be inferred from the reference fields, i.e. the fields without any etched topography, and it is consistent with the results obtained on bare silicon wafers.
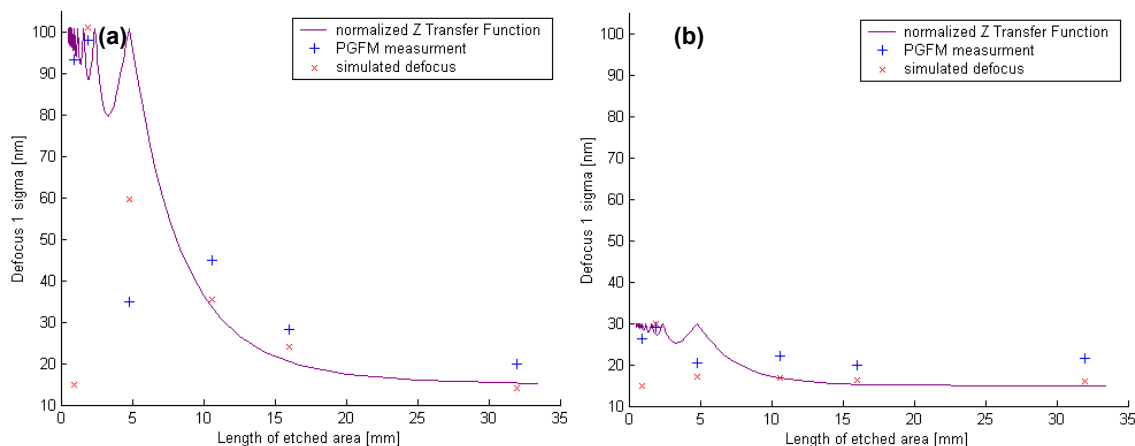

Figure 11 – Measured defocus rms error as a function of the size of the etched areas, along the scan direction, for etch depths of (a) 180 nm and (b) 38 nm. The simulated defocus based on the measured wafer map and the leveling transfer function of the exposure slit is also plotted. Note the significant increase in defocus, as the lateral size of topography gets smaller than approximately 4 mm.

We repeated a similar analysis for a smaller etch-depth of 38 nm, which is more representative of topography encountered in current production environment. Figure 12 shows the comparison between the measured wafer map, the simulated defocus and the defocus data as measured by PGFM, at an identical position on the wafer. The measured performance matches the simulated defocus well.
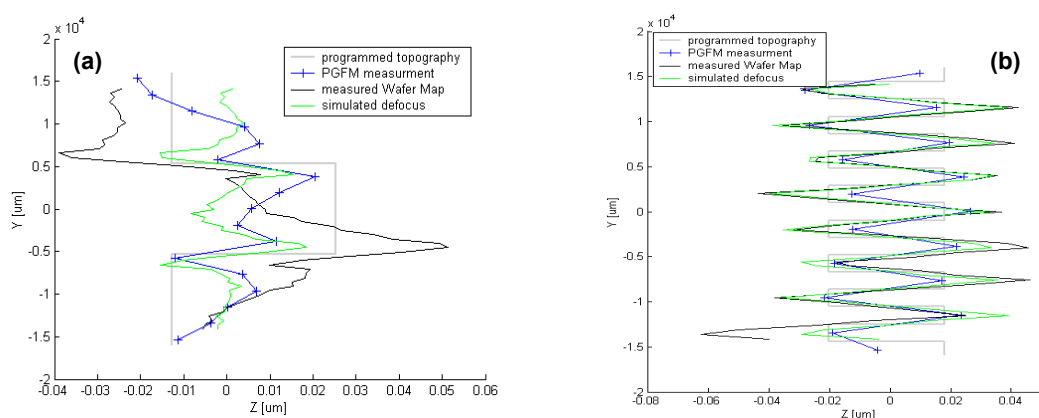

Figure 12 – Comparison of measured defocus along the scan direction with the simulated defocus, for an etch depth of 38 nm. (a) Length of etched area = 10.6 mm. (b) Length of etched area = 1.9 mm.

3.3 Focus control over product-like topography

In this third sub-section, we present some preliminary results on the influence of product-like substrate topography on focus control. In addition to correcting for steps on the wafer surface, as was the case in the previous sub-section, the scanner needs to measure and compensate correctly for topography that may include thin films of various thickness and optical properties. The wafers used for this part of our study were prepared using a source-drain process. The wafer is coated with a thin film and then patterned to define the source and drain areas of a transistor. These areas are then etched away before a thin film of silicon oxide is deposited over the entire wafer. At this point, the wafer is polished to achieve planarity and, finally, a thin film of poly-crystalline silicon is deposited on the wafer. The resulting topography, as measured by a profilometer, is characterized by a height difference of approximately 70 nm between the dense circuit area in the middle of the field and the rest of the field. In figure 13 a contour map of the substrate topography as measured by the TWINSCAN™ AT:1100 is displayed. For each field or chip, there is a step of approximately 80 nm in the center of the field, which agrees well with an independent profilometer measurement result. This topography corresponds probably to polishing errors.
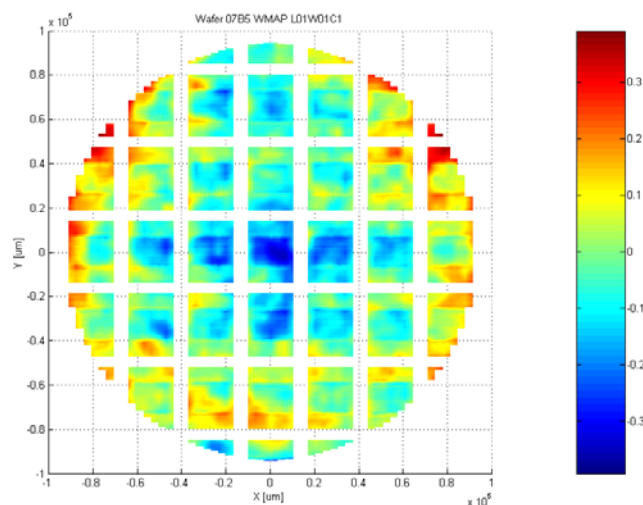

Figure 13 – Wafer topography as measured by the TWINSCAN™ AT:1100. The contour plot of the topography for this product-like wafer is expressed in µm. The height step in the central area of each field is about 80 nm, which is in good agreement with independent profilometer measurements.

We then expose a PSFM reticle over this topography and measure the resulting defocus maps. The results are shown in figures 14 and 15. The whole wafer distribution of defocus data is plotted in figure 14 and is characterized by a 28-nm standard deviation, which represents about a 40% increase in defocus relative to a good quality, bare silicon wafer. This value can also be compared with the results obtained on wafers with programmed topography where a 178-nm etch depth over a large area resulted in an rms defocus error of 35-nm to 40-nm.
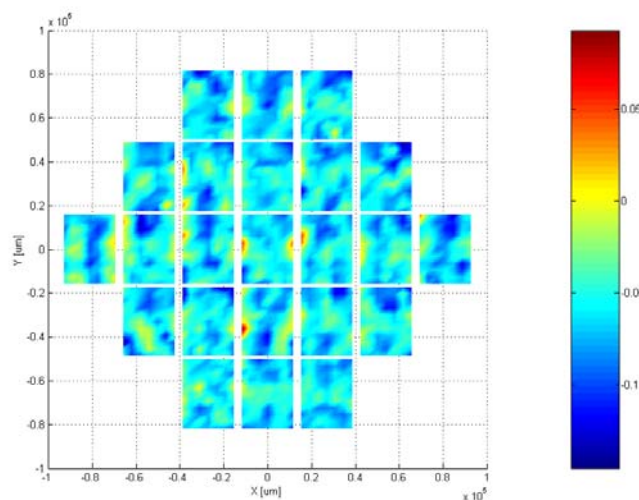
Figure 14 – Defocus distribution over the whole wafer as measured by PSFM, obtained on a product-like wafer. The color bar on the right side of the figure indicates the defocus expressed in microns.

The average-field distribution of defocus is plotted in figure 16. A contour map in the center of the figure shows the distribution of focus offset resulting from the particular topography used here. The location of the dense circuit patterns is indicated on the contour map by a dashed line. On the left of the figure is a lineout of the defocus along the slit direction, averaged over the circuit area. It indicates an average focus shift of approximately 40 nm between the central part of the chip and the periphery.
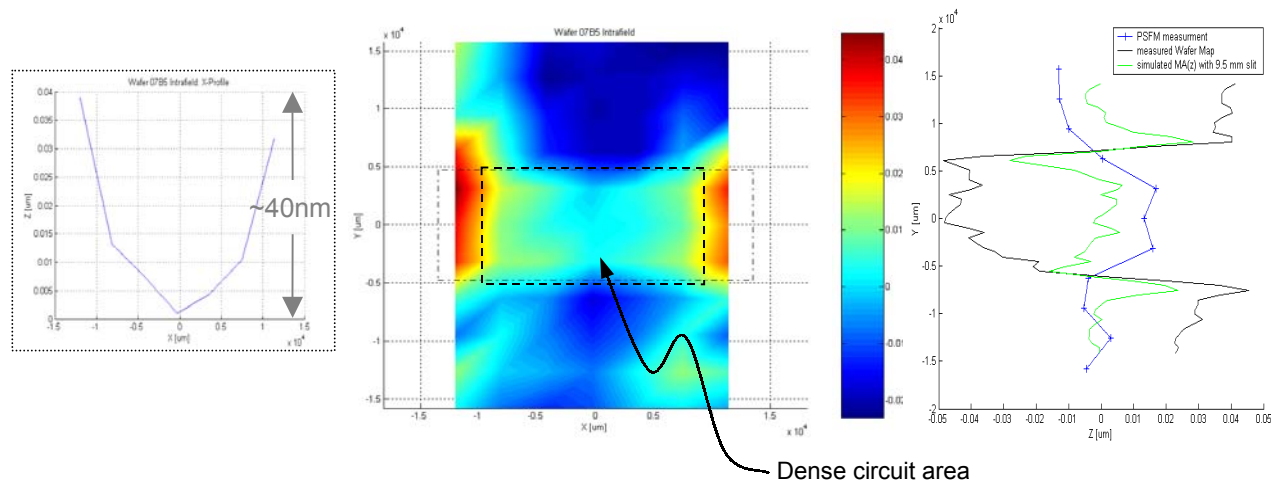

Dense circuit area

Figure 15 – Contour map of the average-field distribution of defocus resulting from the particular topography used here. A lineout of the defocus along the scan direction averaged over the slit direction shown on the right indicates an average focus shift of 20 nm to 30 nm between the central part of the chip and the periphery. The topography measured by the TWINSCAN™ AT:1100 is also displayed on the right side, with the simulated defocus profile along the scan. On the left side, a lineout of the measured defocus along the slit direction, in the central area, also shows a focus shift of approximately 30 nm.

The metrology data from the TWINSCAN™ AT:1100 indicates a step height of approximately 80 nm between the dense circuit area and the periphery of the chip. The measured defocus offset, of about 30 nm, is much smaller than the measured step height. The simulated defocus based on the scanner metrology has an intermediate value of about 60 nm. The discrepancy between the measured defocus step and the predicted performance might be due to calibration errors associated with the use of a slightly different dose and different anti-reflective coating used during the calibration

process. Another source of error is the potential position offset (height offset) of the PSFM structures relative to the surrounding area, due to imperfection in the planarization process. Further investigations are underway to elucidate these results.

4. CONCLUSION

We have used the phase-grating focus monitor (PGFM) and the phase-shift focus monitor (PSFM) to assess the focus control of a state-of-the-art lithography scanner over substrate topography. The results obtained with wafers of different flatness quality emphasize the importance of strict flatness specifications in order to minimize the impact of the wafer on the overall focus budget. The comparison with other metrology methods and simulated defocus reinforce the confidence in the results obtained with PGFM and in the capability of the lithography scanner and set-up. On good wafers, we showed that the TWINSCAN™ focus control is about 100nm or better. The results obtained over programmed topography agree well with the simulated defocus, based on the data from the metrology stage, and they point to an intrinsic limitation of the tool to correct for topography on scalelength of less than approximately 4 mm, due to its finite slit size. Finally, we have obtained some preliminary results about focus control over realistic substrate topography involving thin film and polish effects. These results are consistent so far with those obtained on substrates with programmed topography, which would indicate that thin-film optical effects do not impact focus control significantly. More data and analyses are required to assess focus control over substrates used throughout the fabrication process of a semiconductor device.

ACKNOWLEDGMENTS

REFERENCES

1. H.J. Levinson and W.H. Arnold, "Focus: The Critical Parameter for Submicron Lithography", J.Vac.Sci.Technol.B**5** (1987), pp. 293-298.
2. W.H. Arnold and H.J. Levinson, "Focus: The Critical Parameter for Submicron Lithography, Part 2", Proc. SPIE, Vol.772 (1987), pp.21-34.
3. T.A. Brunner, "New focus metrology technique using special test mask", OCG Interface '93, Sept. 26, 1993, San Diego, CA. Reprinted in Microlithography World, **3** (1) (Winter 1994), pp. 5-13.
4. T.A. Brunner, A.L. Martin, R.M. Martino, C.P. Ausschnitt, T.H. Newman, "Quantitative stepper metrology using the focus monitor test mask", Proc. SPIE, Vol.2197 (1994), pp.541-549.
5. Benchmark Technologies, 7 Kimball Lane, Building E, Lynnfield MA 01940 USA, http://www.benchmarktech.com (US Patent Number 5,300,786 [1994])
6. B. La Fontaine, M. Dusa, J. Krist, A. Acheta, J. Kye, H.J. Levinson, C. Luijten, E. Rodriguez, C. Sager, J. Thomas, J. Van Praagh, "Analysis of Focus Errors in Lithography using Phase-Shift Monitors", in *Optical Microlithography XV*, Anthony Yen, Editor, Proceedings of SPIE Vol. 4691, 315-324 (2002)
7. H. Nomura, "New phase shift gratings for measuring aberrations", Proc. SPIE, Vol.4346 (2001), pp.25-35
8. R. Rubingh, Y. v. Dommelen, S. Tempelaars, M. Boonman, R. Irwin, E. v. Donkelaar, H. Burgers, G. Savenije, B. Koek, M. Thier, O. Römpp, C. Hembd-Söllner, "Performance of a High Productivity 300 mm Dual Stage 193nm 0.75 NA TWINSCAN™ AT:1100 System for 100 nm Applications", ML 4691-70 SPIE 2002
9. The Weir software is distributed by TEA Systems and Benchmark Technologies, http://www.benchmarktech.com